Electronic Supplementary Material (ESI) for ChemComm.

Electrocatalytic ethylbenzene valorization by polyoxometalate @covalent triazine framework using water as oxygen source

Zhen Li, [a] Chengpeng Liu, [a] Weijie Geng, [a] Jing Dong, [b] Yingnan Chi*[a] and Changwen Hu [a]

a. Key Laboratory of Cluster Science Ministry of Education, Beijing Key Laboratory of Photoelectroic/Electrophotonic Conversion Materials, School of Chemistry and Chemical Engineering, Beijing Institute of Technology, Beijing, 100081, People's Republic of China. E-mail: chiyingnan7887@bit.edu.cn.

b. College of Chemistry and Materials Engineering, Beijing Technology and Business University (BTBU), 11 Fucheng Road, Beijing 100048, China

1. Materials and Methods

All the starting materials and organic solvents were purchased from commercial suppliers and used without further purification unless otherwise noted. $H_5PMo_{10}V_2O_{40}\cdot nH_2O$[1] and 1,3-bis(4-cyanophenyl)imidazolium chloride[2] were prepared according to literature methods. Powder X-ray Diffraction (PXRD) was performed on SHIMADZU XRD-6000 X-ray diffractometer equipped with graphite monochromatized Cu Kα radiation (λ = 0.154056 nm). The morphology and microstructure of the samples were observed using transmission electron microscope (TEM, Talos F200X, ThermoFisher Scientific). The FT-IR spectra were collected on a Nicolet 170SXFT-IR spectrophotometer in the range of 400–4000 cm^{-1}. N_2 adsorption desorption isotherms were obtained at 77 K by using a Belsorp max surface area detection instrument and the pore size distribution were calculated. The XPS spectra of the samples were recorded on a Thermo ESCALAB 250Xi. The UV-vis spectra were measured on a UV-2600. Inductively coupled plasma mass spectrometry (ICP-MS) was performed on a Thermo Scientific iCAP Q. Gas chromatograph analyses were performed on a Shimadzu GC-2014C instrument with an FID detector equipped with an HP-5 ms capillary column. The hydrogen evolved was determined using a Techcomp GC-9700 gas chromatograph with a 5 Å molecular sieve column (2 m × 2 mm) and a thermal conductivity detector (TCD). Temperature programmed desorption of ammonia (NH_3-TPD) of $PMo_{10}V_2$@CTF and CTF were tested on a PCA-1200. Initially, 10 mg of $PMo_{10}V_2$@CTF was dried at 120 °C for 30 min under an Ar flow. Then, at a flow rate of 30 mL min^{-1}, the sample was flushed with NH_3 at 80 °C for 30 min. After removing physically adsorbed NH_3 by flowing Ar at 80 °C for 30 min, the chemically adsorbed ammonia was determined by using a thermal conductivity detector (TCD) under the conditions of heating at 10 °C min^{-1} up to 300 °C and then it was kept for 60 min. The GC-MS spectra were obtained using an Agilent 7890A-5975C instrument. The Zeta potential measurements of CTF and $PMo_{10}V_2$@CTF with different feed ratio in aqueous solution using nano particle size and zeta potential analyzer (Zetasizer Nano).

2. Synthesis

Synthesis of the CTF

The cationic CTF was synthesized according to the reported ionothermal method[3]. In a typical experiment, a mixture of 0.613 g (2 mmol) of 1,3-bis(4-cyanophenyl)imidazolium chloride and 1.363 g (10 mmol) of desiccated $ZnCl_2$ was placed into a quartz ampule under an inert atmosphere. The ampule was then evacuated, flame-sealed and transferred into a furnace for heating treatment at 500 ºC for 40 h. The solid monolith obtained was subsequently ground and then washed thoroughly with water to remove most of the $ZnCl_2$. Further stirring in 0.1 M HCl for 12 h was carried out to remove the residual salt. The resulting black powder was washed successively with water and THF and dried in a vacuum at 120 ºC for 12 h.

Synthesis of POM@CTF

The POM@CTF was synthesized according to our previously reported method by the electrostatic assembly of POM and cationic CTF.[4] POM (0.017g, 0.25 g, 0.05 g, or 0.1 g) was dissolved in deionized water (15 mL) and then the CTF (0.1 g) was added. The mixture was stirred at room temperature for 8 h and during the process the characteristic color of POM gradually disappeared. Finally, a black solid of POM@CTF was obtained water washing with a large amount of deionized water and drying at 80 ºC for 12 h.

3. Electrochemical oxidation of EB

Preparation of the POM@CTF electrode.

The POM@CTF working electrode was prepared as follows: POM@CTF (5 mg) was dispersed in isopropanol (1

mL) containing 5 wt% Nafion under ultrasonic conditions. 50 μL of this suspension was drop-cast onto a piece of carbon cloth (1 cm^2) and then dried under vacuum.

Electrochemical measurements.

Voltammetric experiments were performed in anhydrous acetonitrile (10 mL) containing supporting electrolyte $LiClO_4$ (1.5 mmol) at room temperature. All potentials were measured using an Electrochemical Analyzer (Ivium-OctoStat30) with a scan rate of 50 mV s^{-1}. The CV tests of homogeneous $PMo_{10}V_2$ (0.1 mM) were performed using a three-electrode setup with a carbon cloth (CC) as working electrode (1 cm^2), a platinum plate (1 cm^2) electrode as the counter electrode and $Ag/AgNO_3$ as the reference electrode. The CV tests of $PMo_{10}V_2$@CTF were performed with $PMo_{10}V_2$@CTF modified carbon cloth as the working electrode (1 cm^2 effective area), platinum foil as the counter electrode and $Ag/AgNO_3$ electrode as the reference electrode. Electrochemical impedance spectroscopy (EIS) measurements were performed at different potentials from 10^5 to 0.1 Hz.

Bulk electrolysis experiments were performed in an undivided cell using a three-electrode setup with a $PMo_{10}V_2$@CTF-modified carbon cloth (1.0 cm^2) as the working electrode, platinum foil as the counter electrode, and $Ag/AgNO_3$ electrode as the reference electrode. To the cell was added 10 mL of acetonitrile solution containing $LiClO_4$ (1.5 mmol), EB (0.2 mmol) and a potential of 1.6 V vs. $Ag/AgNO_3$ was applied. At the end of electrolysis, biphenyl as the internal standard was added into the reaction solution and the products were qualitatively analyzed by GC. For the recycle test, after the reaction the working electrode, $PMo_{10}V_2$@CTF-modified carbon cloth, was gently washed with acetonitrile and ethyl alcohol three times, dried and used for the next cycle.

Kinetic isotope effect (KIE) of the electrocatalytic oxidation was investigated using d_{10}-ethylbenzene. To the cell was added 10 mL of acetonitrile solution containing $LiClO_4$ (1.5 mmol), EB-d_{10} (0.2 mmol) and a potential of 1.6 V vs. $Ag/AgNO_3$ was applied. At the end of electrolysis, biphenyl as the internal standard was added into the reaction solution and the products were qualitatively analyzed by GC. The k_H/k_D value is calculated by the ratio of the conversion of EB to EB-d_{10}.

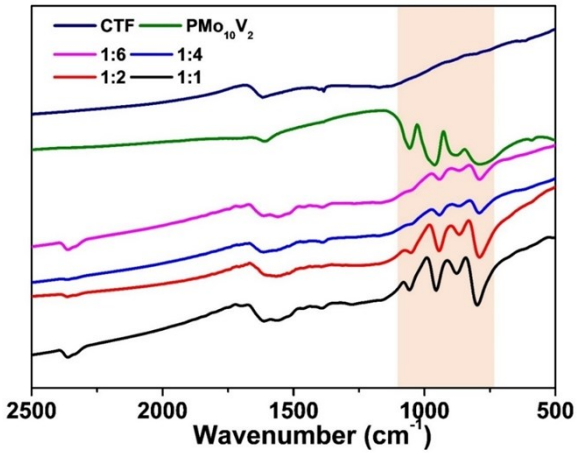

Fig. S1. FT-IR spectra of CTF, $PMo_{10}V_2$ and $PMo_{10}V_2$@CTF prepared by using different feed ratio (m_{POM}:m_{CTF}). The $PMo_{10}V_2$@CTF (1:1, 1:2, 1:4 and 1:6) composites have all characteristic peaks of CTF and $PMo_{10}V_2$, demonstrating the successful immobilization of $PMo_{10}V_2$ on CTF. The characteristic peaks of $PMo_{10}V_2$ including 1049 cm^{-1} for P–O_a (a: tetrahedral oxygen atoms), 945 cm^{-1} for M=O_d (d: terminal oxygen atoms), 877 cm^{-1} for M–O_b–M (b: corner shared oxygen atoms), and 771 cm^{-1} for M–O_c–M (c: edge-shared oxygen atoms) can be observed in the FT-IR spectra of $PMo_{10}V_2$@CTF (1:1, 1:2, 1:4 and 1:6). Compared with pristine $PMo_{10}V_2$, the vibration of M–O_c–M undergoes a slight red shifts, implying the electrostatic interaction between POM and CTF.

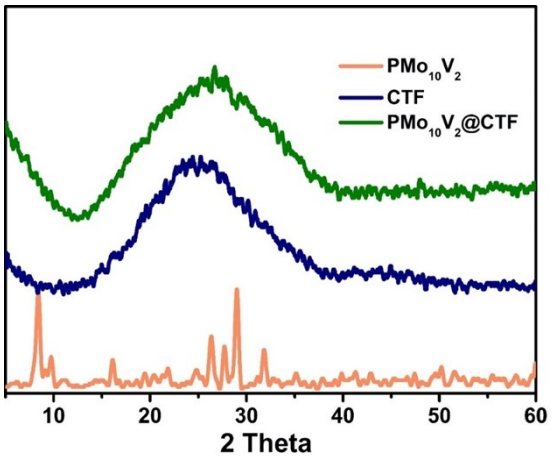

Fig. S2. PXRD patterns of $PMo_{10}V_2$, CTF, and $PMo_{10}V_2$@CTF (1:2). The observation of a broad peak reveals that $PMo_{10}V_2$@CTF is amorphous and there is no characteristic diffraction peak of $PMo_{10}V_2$, showing that $PMo_{10}V_2$ is well dispersed on the support.

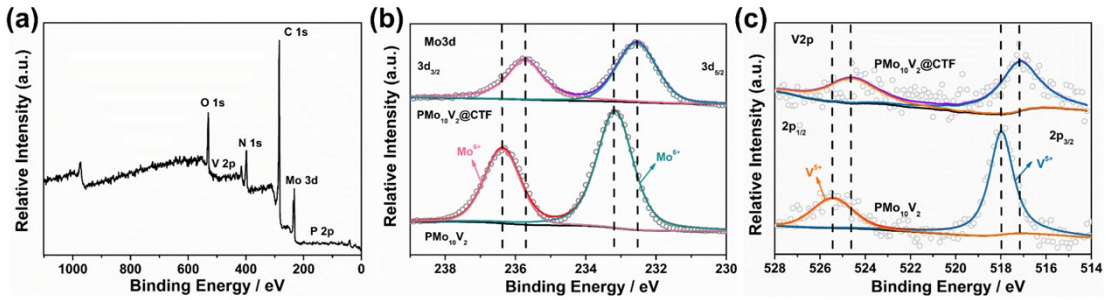

Fig. S3. XPS spectra of a survey scan of $PMo_{10}V_2$@CTF (a); XPS spectra Mo 3d (b) and V 2p (c) of $PMo_{10}V_2$ and $PMo_{10}V_2$@CTF. We can clearly observe the Mo 3d, and V 2p signals in the XPS spectrum of $PMo_{10}V_2$ (Fig. S3a). As shown in Fig. S3b, in $PMo_{10}V_2$@CTF the peaks at 236.4 eV (Mo $3d_{3/2}$) and 233.2 eV (Mo $3d_{5/2}$) are assigned to the Mo^{6+} oxidation state. In the V 2p region (Fig. S3c), two peaks at 525.4 eV (V $2p_{1/2}$) and 518.0 eV (V $2p_{3/2}$) confirm the V^{5+} oxidation state in the composite. It is found that after immobilization the binding energies of both Mo 3d and V 2p in the $PMo_{10}V_2$@CTF composite move to the lower region. The shift of binding energy (about 0.7 eV) indicates that the electron of CTF partly transfer to $PMo_{10}V_2$ during the electrostatic assembly process and the electron transfer from CTF to $PMo_{10}V_2$ leads to the increase of electron density around Mo and V centers. Similar phenomenon has been observed in our previous investigation. [4] The electrostatic interactions between $PMo_{10}V_2$ and CTF might contribute to electron transfer in electrocatalytic oxidation.

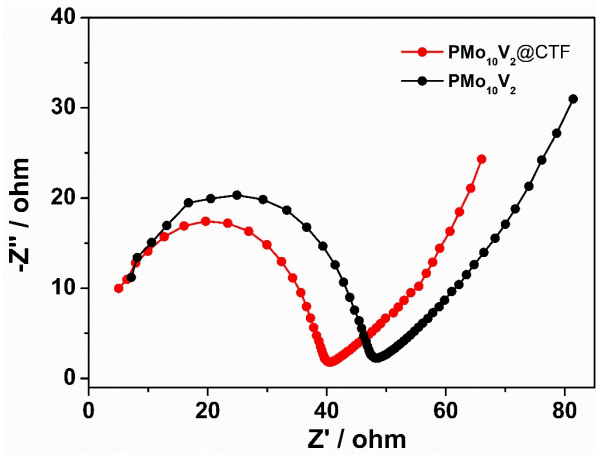

Fig. S4. Nyquist plots of the pristine $PMo_{10}V_2$ and $PMo_{10}V_2$@CTF catalysts in acetonitrile solution containing $LiClO_4$ (1.5 mmol).

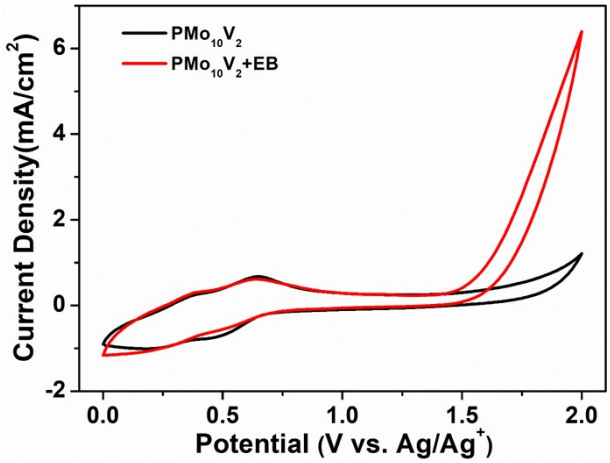

Fig. S5. The cyclic voltammograms (CV) of 0.1 mM $PMo_{10}V_2$ acetonitrile solution containing $LiClO_4$ (1.5 mmol) in the absence or presence of EB using carbon cloth as working electrode with a scan rate of 50 mV s^{-1}.

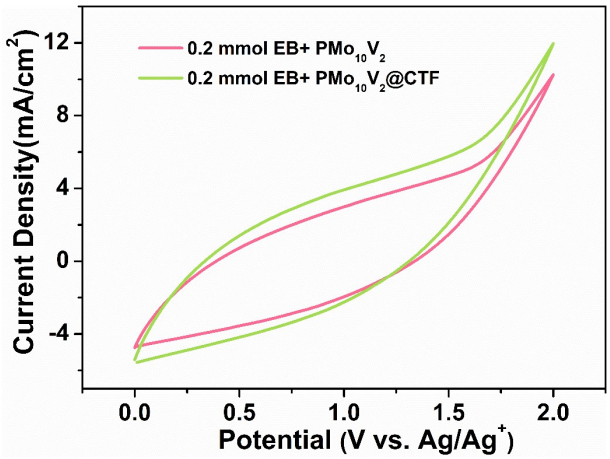

Fig. S6. The cyclic voltammograms (CV) of acetonitrile solution containing $LiClO_4$ (1.5 mmol) and EB (0.2 mmol) using homogeneous $PMo_{10}V_2$ and heterogeneous $PMo_{10}V_2$@CTF as electrocatalysts, respectively and in both cases the $PMo_{10}V_2$ amount is about 0.07 mg.

Fig. S7. Undivided cell used for bulk electrolysis reactions.

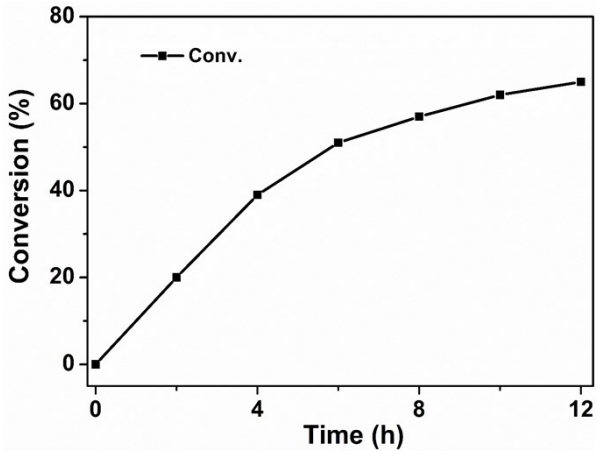

Fig. S8. Time profile for the electrocatalytic oxidation of EB.

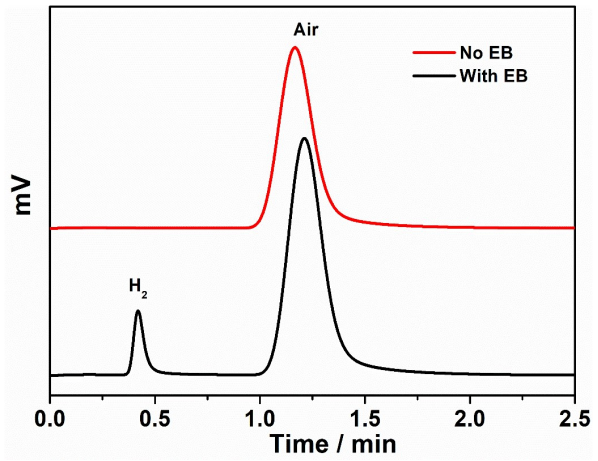

Fig. S9. The gas chromatograph of EB oxidation with and without EB. To the cell was added 10 mL of acetonitrile solution containing $LiClO_4$ (1.5 mmol), EB (0.2 mmol) and a potential of 1.6 V vs. $Ag/AgNO_3$ was applied. The undivided cell was sealed and a small amount of hydrogen gas was generated over time at the cathode part. After the reaction, 100 μL gas was extracted from the cell and injected into gas chromatograph (SHIMADZU-GC2014C) for qualitative analysis, equipped with a thermal conductivity detector and a TDX-01 packed column. Argon was used as a carrier gas. The peak at 0.38 min is attributed to H_2. Compared with the experiment without adding EB, it is found that there is no H_2 production. Therefore, we can conclude that the origin of H_2 is produced by electrolytic conversion of ethylbenzene.

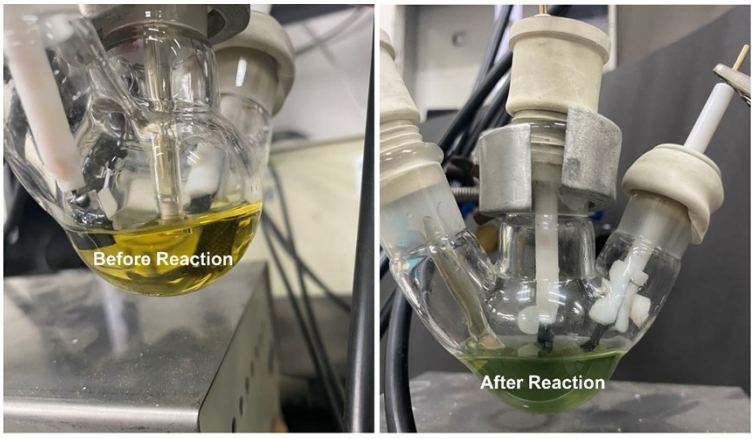

Fig. S10. The images before and after the EB oxidation reaction using homogeneous $PMo_{10}V_2$ as electrocatalyst. After the electrochemical oxidation, the reaction solution changed from yellow to green, indicating that $PMo_{10}V_2$ was reduced during the electrocatalytic process.

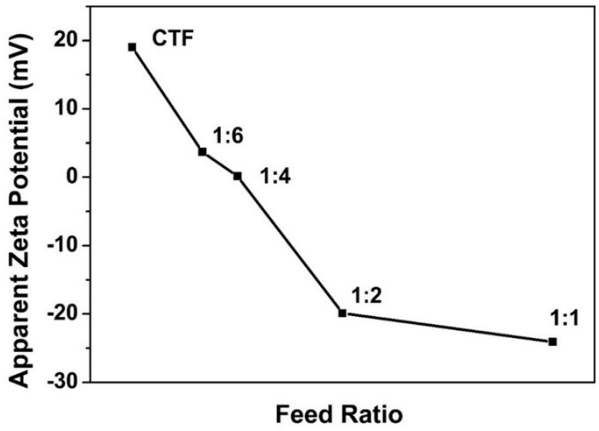

Fig. S11. Zeta potential (mV) measurements of CTF and $PMo_{10}V_2$@CTF with different feed ratio in aqueous solution (5 mg/mL). The zeta potential of CTF is +19 mV, indicating the surface of the CTF is positively charged. With the increase of $PMo_{10}V_2$ feeding amounts, an obvious decrease of zeta potential was observed from +3.2 mV (1:6 $PMo_{10}V_2$@CTF) to -19.9 mV (1:2 $PMo_{10}V_2$@CTF), showing the successful immobilization of polyanions on the surface of CTF. However, when the feed ratio reaches 1:1, the downtrend of zeta potential is signifcantly weakened, revealing that the immobilization of POM is nearly saturated.

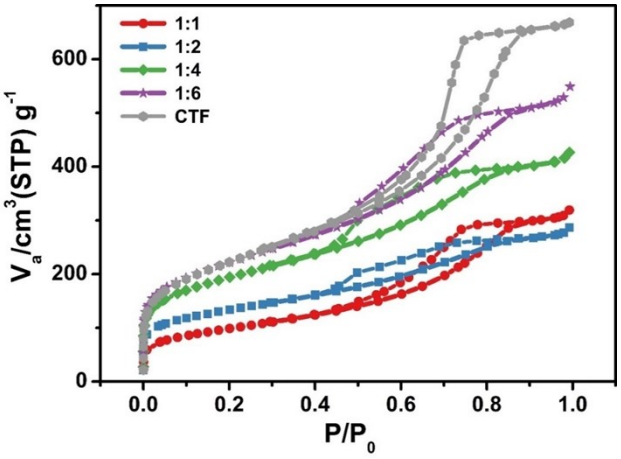

Fig. S12. N_2 adsorption and desorption isotherms for CTF and $PMo_{10}V_2$@CTF (1:6, 1:4, 1:2 and 1:1) measured at 77 K.

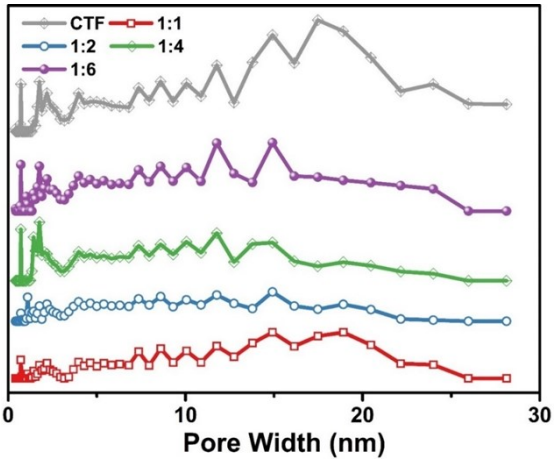

Fig. S13. The pore size distributions (PSD) curves of CTF and $PMo_{10}V_2$@CTF (1:1, 1:2, 1:3 and 1:4).

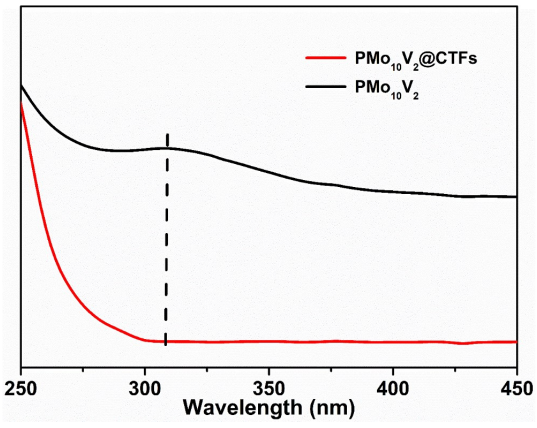

Fig. S14. Liquid-phase UV-Vis spectra from leaching test of $PMo_{10}V_2$@CTF (1:2). To confirm the heterogeneity of $PMo_{10}V_2$@CTF electrocatalyst, the composite was soaked in acetonitrile and there is no characteristic absorption of $PMo_{10}V_2$ detected in the soaking solution.

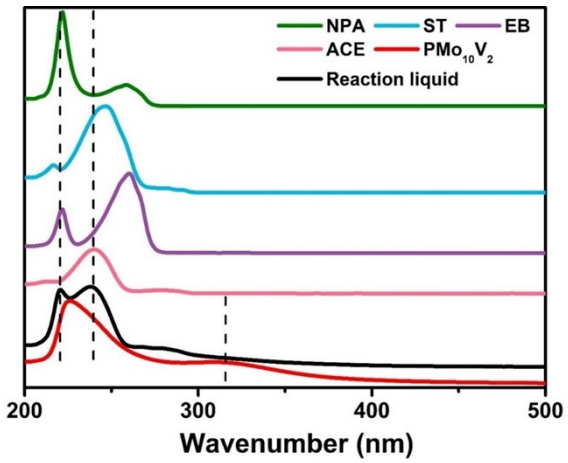

Fig. S15. UV-Vis spectra of postreaction, ST, ACE, NPA and $PMo_{10}V_2$ solutions. For the post-reaction solution, no characteristic absorption of $PMo_{10}V_2$ was detected from the UV-vis spectrum.

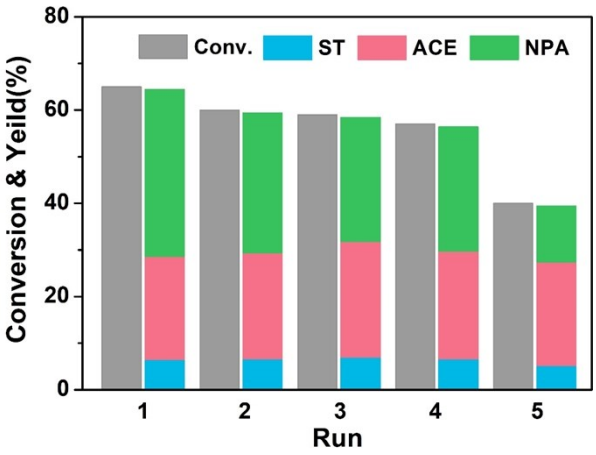

Fig. S16. Recycle test for the electrocatalytic oxidation of EB by $PMo_{10}V_2$@CTF (1:2).

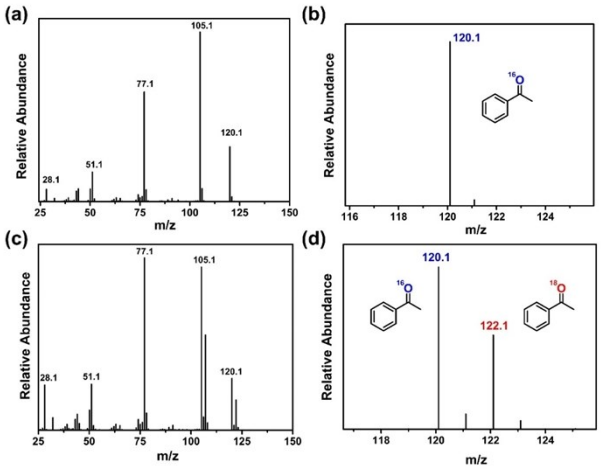

Fig. S17. GC-MS spectra of ACE generated from the EB oxidation by $PMo_{10}V_2$@CTF. The isotopic distribution patterns without adding $H_2{}^{18}O$ (a and b) and with adding $H_2{}^{18}O$ (c and d).

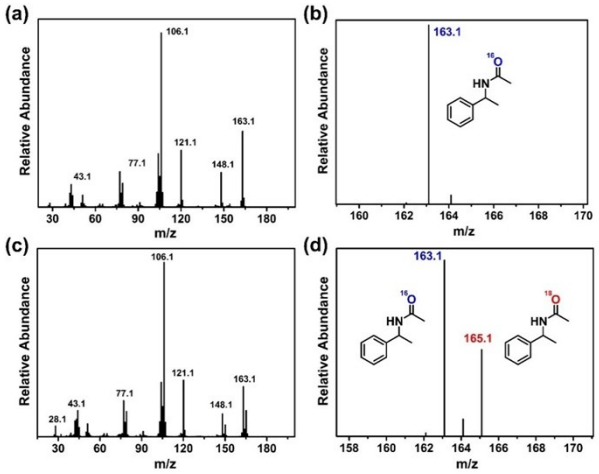

Fig. S18. GC-MS spectra of NPA generated from the EB oxidation by $PMo_{10}V_2$@CTF. The isotopic distribution patterns without adding $H_2{}^{18}O$ (a and b) and with adding $H_2{}^{18}O$ (c and d).

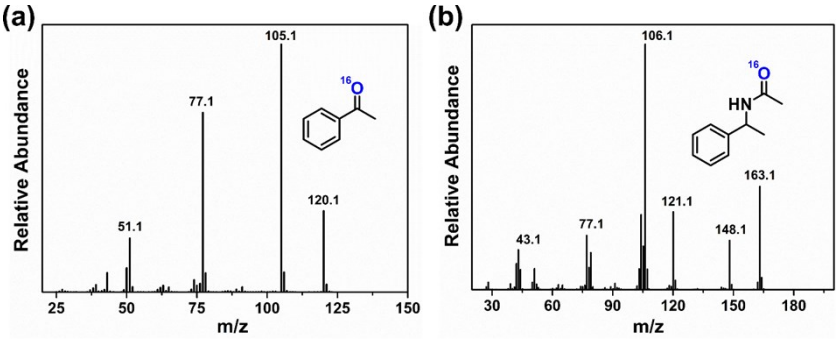

Fig. S19. The isotopic distribution patterns of ACE and NPA with adding $H_2{}^{18}O$ under the turnover conditions (a and b).

Control experiment confirms that ACE and NPA does not exchange O with $H_2{}^{18}O$ under the turnover conditions and so the generation of ^{18}O-labeled ACE and NPA strongly supports the oxygen source is from to H_2O. The ^{16}O-ACE peak originates from the H_2O of $LiClO_4$.

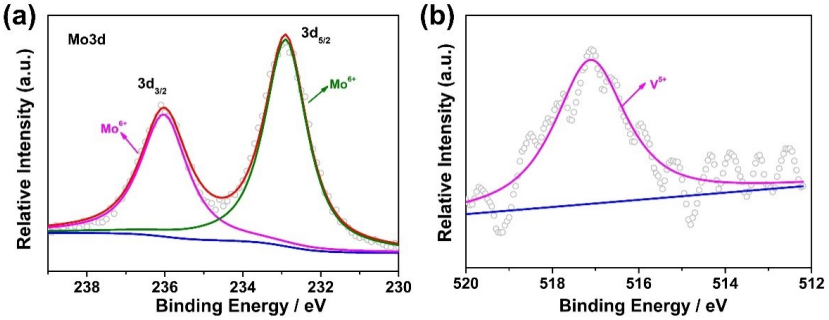

Fig. S20. XPS spectra of $PMo_{10}V_2$@CTF (a) Mo 3d and (b) V 2p after EB oxidation. The XPS spectrum of the recycled catalyst was also measured, where the V 2p and Mo 3d peaks are basically unchanged relative to the fresh sample. The Mo 3d peaks could be deconvoluted into 236 eV ($3d_{3/2}$, Mo^{6+}), 232.9 eV ($3d_{5/2}$, Mo^{6+}), and the V $2p_{3/2}$ peak could be deconvoluted into 517.1 eV (V^{5+}). The XPS analyses imply that $PMo_{10}V_2$@CTF remains stable after the electrocatalytic oxidation and the Mo and V centers are still in their highest oxidation state.

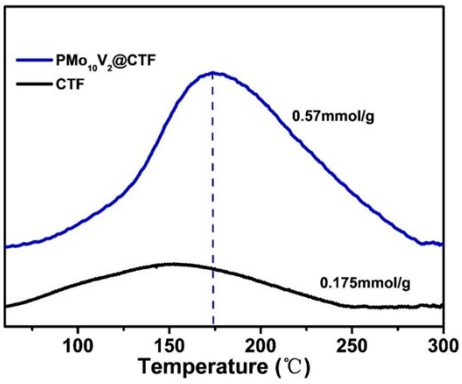

Fig. S21. NH_3-TPD of $PMo_{10}V_2$@CTF and CTF. The absorption peaks between 100 °C and 250 °C correspond to weak acid sites and the total acidity capacity of $PMo_{10}V_2$@CTF is calculated to be 0.57 mmol g^{-1} which is higher than that of CTF (0.175 mmol g^{-1}), indicating that $PMo_{10}V_2$@CTF has weak Brønsted acidity.

Table S1. Electrochemical oxidation of ethylbenzene under different reaction conditions.

Catalyst	Working electrode	Additives/ Oxidants	Conditions, Time	Conv. (%)	Product (Yield, %)	FE (%)	Ref.
$PMo_{10}V_2$@CTF	CC	none	1.6 V, 12 h	65	ST (6.5), ACE (22.1), NPA (35.8)	90.4	This work
none	Pt	none	20 mA, 5 h	-	ACE (49)	54	5
none	-	MSA [a]	200 mA, 9 h	-	NPA (64)	-	6
$K_5Co^{III}W_{12}O_{40}$	Pt	AcOH	1.8 V, 3 h	20	ST (13.4), ACE (6.6)	21	7
none	RVC [b]	*t*BuOOH	1.1 V, 15 h	-	ACE (56)	-	8
Ru-based complex [c]	nanoITO	none	1.74 V, 12 h	-	-	95	9
Fe-based complex [d]	RVC	none	1.25 V, 10 h	92	ACE (79)	-	10
none [f]	Pt	none	2.17 V	-	NPA (51)	-	11
Ru-CTF	CP	none	1.5 V, 12 h	-	-	24	12

a: MSA: methanesulfonic acid;

b: RVC: 100 PPI Reticulated Vitreous Carbon;

c: $[Ru(Mebimpy)(4,4'-((HO)_2OPCH_2)_2bpy(OH_2)]^{2+}$, nanoITO: nanocrystalline Sn(IV)-doped In_2O_3;

d: $(TAML)Fe^{III}–OH_2$ complex, (TAML = tetraamido macrocyclic ligand);

Compared with the previous reports in the electrochemical oxidation of EB (see Table S1), the electrocatalytic oxidation in this work exhibits the following advantages. First, 65% of EB was converted by $PMo_{10}V_2$@CTF under ambient conditions and 90.4% of Faraday efficiency (FE) was achieved. However, only 20% of EB was converted by homogeneous $K_5CoW_{12}O_{40}$ (25%) using Pt as working electrode.[7] Although the conversion of EB was as high as 92% by homogeneous Fe(TAML) complex (10%), the catalyst is unstable under the turnover conditions and the value of FE was not mentioned. Second, a noble metal free working electrode, $PMo_{10}V_2$@CTF, was used in our reaction instead of Pt or Ru-based working electrodes. Third, the electrochemical oxidation by $PMo_{10}V_2$@CTF does not require using additional additives (such as strong acids) and oxidants, and water is the only oxygen source. By comparison, the catalytic oxidation in our work is much greener. Finally, $PMo_{10}V_2$@CTF can be reused for three time without substantial loss of catalytic activity. In comparison, the recyclability was not documented in the reported catalytic systems.

Table S2. Electrocatalytic oxidation of EB using different catalysts.

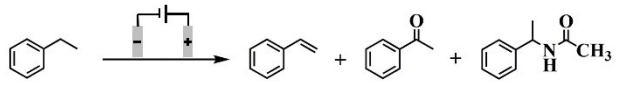

EB ST ACE NPA

Entry	Catalysts	Conv.	Yield of ST	Yield of ACE	Yield of NPA	FE
1	CTF	27%	1.4%	5.7%	11%	21.3%
2	$PMo_{10}V_2$@CTF (1:6)	32%	8.6%	15%	3.9%	56.1%
3	$PMo_{10}V_2$@CTF (1:4)	50%	8.7%	25%	16%	72.8%
4	$PMo_{10}V_2$@CTF (1:2)	65%	6.5%	22%	36%	90.4%
5	$PMo_{10}V_2$@CTF (1:1)	51%	7.7%	15%	4.6%	54.4%
6	PW_{12}@CTF (1:2)	45%	7.2%	21%	15%	61.0%
7	PMo_{12}@CTF (1:2)	48%	9.6%	21%	13%	61.1%
8	$PMo_{10}V_2$ + CTF [a]	44%	11%	8.8%	20%	59.5%
9	$Cs_5PMo_{10}V_2$ [b]	54%	8.1%	27%	N. D.	48.0%
10	$Cs_5PMo_{10}V_2$+CTF [c]	62%	11%	30%	N. D.	40.5%

Reaction conditions: To the cell was added 10 mL of acetonitrile solution containing $LiClO_4$ (1.5 mmol), EB (0.2 mmol) and a potential of 1.6 V vs. $Ag/AgNO_3$ was applied. At the end of electrolysis, biphenyl as the internal standard was added into the reaction solution and the products were qualitatively analyzed by GC. N.D. is denoted as not detected.

a: The oxidation of EB was performed using homogeneous $PMo_{10}V_2$ as electrocatalyst combined with CTF modified carbon cloth as electrode (denoted as $PMo_{10}V_2$ + CTF in Figure 2b), where the amount of $PMo_{10}V_2$ and CTF is identical to that of $PMo_{10}V_2$@CTF (1:2).

b: The electrocatalytic oxidation of $Cs_5PMo_{10}V_2O_{40}$, an insoluble salt of $PMo_{10}V_2$, was evaluated and amount of POM is identical to that of $PMo_{10}V_2$@CTF (1:2).

c: The EB oxidation using the mechanical mixture of $Cs_5PMo_{10}V_2O_{40}$ and CTF with a ratio of 1:2, was evaluated and amount of POM and CTF is identical to that of $PMo_{10}V_2$@CTF (1:2).

Notably, $PMo_{10}V_2$ + CTF only converted 44% of EB and the total yield of three products (ST:11%, ACE: 8.8%, NPA: 20%) is 40% (Table S2, entry 8). In comparison, $PMo_{10}V_2$@CTF (1:2) (Table S2, entry 4) converted 65% of EB and the total yield of three products (ST:6.5%, ACE: 22%, NPA: 36%) is 65%.The above results indicate that CTF supported $PMo_{10}V_2$ exhibits better electrocatalytic activity than homogeneous $PMo_{10}V_2$. The possible reasons are as follows. (i) the stability of $PMo_{10}V_2$ (main catalytic sites) is enhanced after combining with CTF. After the EB oxidation, the reaction solution containing homogeneous $PMo_{10}V_2$ changed from yellow to green (Figure S10), showing that $PMo_{10}V_2$ was reduced during the electrocatalytic process. By contrast, the XPS measurement implies that the oxidation states of V and Mo are basically unchanged after the electrocatalytic reaction (Figure S20). (ii) Electrochemical impedance spectroscopy (EIS) measurements (Figure S4) demonstrate that the conductivity of $PMo_{10}V_2$@CTF is much better than that of pristine $PMo_{10}V_2$ and that would enhance the electron transfer efficient during the electrochemical oxidation. (iii) The CTF support with well-distributed pores contributes to the even dispersion of POMs, providing more accessible active sites. This part has been discussed in detail in the main text using the $PMo_{10}V_2$@CTF (1:6, 1:4, 1:2 and 1:1) as a platform. (iv) The immobilization of catalyst on electrode surfaces will promote electronic communication with the electrode. In the homogeneous electrocatalytic system, the turnover of $PMo_{10}V_2$ only occurs when it diffuses to the surface of electrode. However, when $PMo_{10}V_2$ is immobilized on the CTF used as electrode material, turnover frequency of $PMo_{10}V_2$ will be improved in some

degree.

As shown in Table S2, entry 9, the direct use of $Cs_5PMo_{10}V_2O_{40}$ as catalytic electrode can convert 54% of EB but no NPA (the main product by $PMo_{10}V_2$@CTF (1:2)) was detected. And the total yield of ST and ACE is 35%, and the total Faraday efficiency (48%) is much less than that of $PMo_{10}V_2$@CTF (90.4%). As shown in Table S2, entry 10, the conversion by the mixture of $Cs_5PMo_{10}V_2O_{40}$ and CTF (62%) is close to that of $PMo_{10}V_2$@CTF (1:2) (65%), but still only ST (yield:11%) and ACE (yield: 30%) were obtained with a lower Faraday efficiency (40.5%). The above two control experiments reveal that (i) the $PMo_{10}V_2$ polyanion is the main catalytic active sites in the EB oxidation; (ii) the electrostatic interaction of $PMo_{10}V_2$ and CTF plays an important role for the formation NPA. We speculate that the $PMo_{10}V_2$ clusters are evenly dispersed on the support in $PMo_{10}V_2$@CTF (1:2) and the accessible $PMo_{10}V_2$ can efficiently stabilize the formed carbocation intermediate, which can be subsequently attacked by acetonitrile giving NPA. However, when insoluble $Cs_5PMo_{10}V_2O_{40}$ with poor conductivity and low surface area was used, the $PMo_{10}V_2$ clusters were surrounded by Cs^+ ions exhibiting poor ability in stabilizing carbocation intermediate and resultingly the carbocation can only be trapped by strong nucleophiles, such as H_2O.

Table S3. Surface area and porosity data of CTF and $PMo_{10}V_2$@CTF (1:6, 1:4, 1:2 and 1:1).

Entry	Catalysts	Surface area ($m^2\ g^{-1}$)	Pore size (nm)	Pore volume ($cm\ g^{-1}$)	loading amount (%) of POM
1	CTF	1154	5.353	1.813	-
2	$PMo_{10}V_2$@CTF (1:6)	780.1	4.312	0.841	12
3	$PMo_{10}V_2$@CTF (1:4)	685.3	3.832	0.657	21
4	$PMo_{10}V_2$@CTF (1:2)	468.5	3.761	0.441	28
5	$PMo_{10}V_2$@CTF (1:1)	348.2	5.644	0.491	32

Table S4. Electrocatalytic activity of EB oxidation under different atmospheres.

Entry	Atmosphere	Conv.	Yield of ST	Yield of ACE	Yield of NPA
1	Air	47%	8%	28%	60%
2	Ar	47%	7%	21%	59%

Reaction conditions: To the cell was added 10 mL of acetonitrile solution containing $LiClO_4$ (1.5 mmol), EB (0.2 mmol) and a potential of 1.6 V vs. $Ag/AgNO_3$ was applied, reaction time 6 h. At the end of electrolysis, biphenyl as the internal standard was added into the reaction solution and the products were qualitatively analyzed by GC.

Table S5. The total Faraday efficiency of each catalytic cycle.

Catalytic cycle	Conv.	Yield of ST	Yield of ACE	Yield of NPA	total Faraday efficiency
1	65	6.5	22.1	35.8	90.4
2	60	6.6	22.8	30	81.8
3	59	7	24.8	26.6	74.5
4	57	6.6	23.1	26.7	71.0
5	40	5.2	22.2	12	85.7

Reference

1. R. Neumann and M. Lissel, *J. Org. Chem.*, 1989, **54**, 4607-4610.
2. R. S. Crees, M. L. Cole, L. R. Hanton and C. J. Sumby, *Inorg. Chem.*, 2010, **49**, 1712-1719.
3. T. T. Liu, R. Xu, J. D. Yi, J. Liang, X. S. Wang, P. C. Shi, Y. B. Huang and R. Cao, *ChemCatChem*, 2018, **10**, 2036–2040.
4. Z. Li, J. Zhang, X. Jing, J. Dong, H. Liu, H. Lv, Y. Chi and C. Hu, *J. Mater. Chem. A*, 2021, **9**, 6152-6159.
5. L. Meng, J. Su, Z. Zha, L. Zhang, Z. Zhang and Z. Wang, *Chem. – Eur. J.*, 2013, **19**, 5542-5545.
6. M. A. Kabeshov, B. Musio and S. V. Ley, *React. Chem. Eng.*, 2017, **2**, 822-825.
7. A. M. Khenkin, M. Somekh, R. Carmieli and R. Neumann, *Angew. Chem. Int. Ed.*, 2018, **57**, 5403-5407.
8. J. A. Marko, A. Durgham, S. L. Bretz and W. Liu, *Chem. Commun.*, 2019, **55**, 937-940.
9. A. K. Vannucci, Z. F. Chen, J. J. Concepcion and T. J. Meyer, *ACS Catal.*, 2012, **2**, 716-719.
10. A. Das, J. E. Nutting and S. S. Stahl, *Chem. Sci.*, 2019, **10**, 7542-7548.
11. T. Tajima, H. Kurihara, A. Nakajima and T. Fuchigami, *J. Electroanal. Chem.*, 2005, **580**, 155-160.
12. S. Kato, K. Iwase, T. Harada, S. Nakanishi and K. Kamiya, *ACS Appl. Mater. Interfaces*, 2020, **12**, 29376-29382.